Invited Paper

# III-nitride deep ultraviolet micro- and nano-photonics

Z.Y. Fan, J.Y. Lin and H.X. Jiang
Department of Physics, Kansas State University, Manhattan, Kansas 66506-2601, USA

## ABSTRACT

Recent progresses in epitaxial growth, fundamental studies of high Al content AlGaN alloys with Si and Mg doping, light polarization properties, and deep UV LEDs combined with microlens or photonic crystal structure to improve light extraction are presented. For Si doped $Al_{0.7}Ga_{0.3}N$, a room temperature *n*-type resistivity as low as 0.0075 Ω·cm has been obtained. We have also achieved *n*-AlN with a free electron concentration and mobility of about $1.0 \times 10^{17} cm^{-3}$ and 2 $cm^2/Vs$, respectively. For Mg doped $Al_{0.7}Ga_{0.3}N$, we have obtained a resistivity around $10^5$ Ω cm at room temperature and confirmed *p*-type conduction at elevated temperatures (> 700 K) with a resistivity of about 40 Ω cm at 800 K. Based on the optimized material growth, 280 nm deep UV LED with forward voltage of 6.7 V, and output power of 0.35 mW has been achieved at 20 mA. To enhance light extraction efficiency, sapphire microlens array was monolithically integrated on flip-chip bonded deep UV LED substrates; a light extraction enhancement of 55% was achieved. To improve the transverse light extraction, photonic crystal structures were incorporated into the devices, and significant light extraction enhancement was achieved.

Keywords: III-nitride wide bandgap semiconductors, DUV LEDs, nano-photonics, *n*-AlGaN, *p*-AlGaN, photonic crystals, light extraction efficiency, light polarization, microlens.

## 1. INTRODUCTION

With the success of GaN semiconductor applications in blue light-emitting diodes (LEDs) and laser diodes, research interest is now being concentrated on the development of wide bandgap AlGaN technology, which covers a wavelength from 360 nm down to 200 nm. In this wavelength range the solid-state ultraviolet (UV) and deep ultraviolet (DUV) LEDs have many critical applications.[1] For examples, protein fluorescence is generally excited by UV light; hence, the availability of chip-scale UV light sources may open new avenues for medical research. The compact UV emitters can be used in a portable instrument for chemical and biological agent detection by fluorescence analysis. The ability of integration of UV emitters and detectors on single chips may also find new applications in biomedical research and disease diagnosis with the development of lab-on-a-chip. By wavelength down-conversion, the chip-scale UV emitters also have a great potential for the solid-state lighting. High intensity and high speed UV LEDs could also be used as transceivers for covert non-line-of-sight (NLOS) optical communications.

With the huge strive to develop AlGaN-based compact UV LEDs, significant progresses are being achieved, and emission wavelength is being pushed down to 250 nm,[2] but the efficiency and power output are still very low. Several major issues have been identified, which have to be addressed before high performance UV emitters can be developed. For deep UV emission with $\lambda \sim 280$ nm, the quantum-well (QW) structure based LED requires an active layer with Al content close to 50%, and invariably, this value for the *p*- and *n*-cladding should be more than that of the active layer. It has been found that the high Al composition not only introduces dislocations that seriously limit the emission efficiency, it also leads to a poor *p*- and *n*-type conductivity in the cladding layers due to the deepening of the impurity levels, limiting the current injection and increasing the operation voltage. Different material structures have been proposed to improve the material quality and the UV LED power level, for example, using short-period superlattice to supply carriers without significant band-gap narrowing,[3] insertion of AlN/AlGaN superlattice as defect filter for the buffer growth,[4] and structure growth on non-polar sapphire plane to eliminate the polarization effect.[5] However, The attainment of highly conductive *p*-type AlGaN (of any Al composition) and *n*-type $Al_xGa_{1-x}N$ alloys (x > 0.7) remain one of the foremost challenging tasks of the Nitride community. Achieving highly conductive *n*-$Al_xGa_{1-x}N$ alloys with high Al contents is very challenging due to an increase in the ionization energy of the dopants and an enhanced compensation of native defects (cation vacancy and cation vacancy-oxygen complex) with an increase of the alloy composition,[6,7] while the effectiveness to achieve *p*-AlGaN with high Al composition by Mg doping is a much more serious problem.

Quantum Sensing and Nanophotonic Devices III, edited by Manijeh Razeghi, Gail J. Brown,
Proc. of SPIE Vol. 6127, 61271C, (2006) · 0277-786X/06/$15 · doi: 10.1117/12.641250

The efficiency of AlGaN-based UV and DUV LEDs also depends on the light extraction. The light extraction is limited by the high refractive index of semiconductor materials to a small extraction cone, with a typical extraction efficiency of less than 5%. Most of the emitted light generated in the LED QW region is confined in the QW and cladding layers and finally absorbed by material defects. How to improve the light extraction efficiency is another critical issue for UV LED development. Recently, the properties of the fundamental optical transitions in AlN have been reported.[8] The band-structure of wurtzite AlN near the $\Gamma$-point was found to be very different from GaN, which gives rise to unique optical properties of AlGaN alloys and their associated UV LEDs. Since these devices are typically surface emitters with light extraction cone along the nitride crystal *c* direction, if the band structure change leads to a change of emission light polarization and propagation direction, the light extraction efficiency could be significantly influenced.

In this paper, we summarize some of our recent progresses in epitaxial growth, fundamental studies and fabrication of nitride DUV materials and devices. Electrical and optical measurements were employed to study the Si and Mg doped AlGaN alloys with high Al content up to pure AlN. Polarization study shows that for $Al_xGa_{1-x}N$ with x>0.25, the light with electrical field *E* parallel to the crystal *c* axis (*E//c*) is the dominant emission in AlGaN materials. With the optimized material growth, we also report the fabrication of our DUV LEDs emitting at 280 nm. To enhance light extraction efficiency limited by refraction, sapphire microlens array was monolithically integrated on flip-chip bonded UV LED substrates; to improve the transverse light extraction, photonic crystal structures are incorporated into the devices fabrication.

## 2. EXPERIMENT

$Al_xGa_{1-x}N$ and AlN epilayers (1 µm thick) were grown on sapphire (0001) substrates with AlN buffer layers by metal organic chemical vapor deposition (MOCVD). The growth temperature and pressure were around 1050 $^oC$ and 50 Torr, respectively. The metal organic sources used were trimethylgallium (TMGa) for Ga and trimethylaluminum (TMAl) for Al, and blue ammonia ($NH_3$) was the gas source for N. Silane ($SiH_4$) and bis-cyclopentadienyl-magnesium ($Cp_2Mg$) were used for Si and Mg doping, respectively. The doping level was varied by controlling the $SiH_4$ and $Cp_2Mg$ flow rates. The Al contents of AlxGa1-xN alloys were determined by energy dispersive x-ray (EDX) and x-ray diffraction (XRD) measurements as well as by the flow rates of TMGa and TMAl. The Al contents determined by all three methods agreed within ±0.02. Secondary ion mass spectroscopy (SIMS) measurements were also performed (by Charles Evan & Associates) for selective samples to verify the Si and Mg dopant concentrations. Atomic force microscopy (AFM) and scanning electron microscopy (SEM) were employed to examine the surfaces and revealed crack-free epilayers. Variable temperature Hall-effect (standard Van der Pauw) measurements were used to measure the electron concentration, mobility, and resistivity of these materials. A deep UV (5 mW @ 197 nm) picosecond time-resolved photoluminescence (PL) spectroscopy system was specially designed to probe the optical properties of materials and device structures based on AlGaN alloys with high Al contents. The deep UV PL system consists of a frequency quadrupled 100 femtosecond Ti:sapphire laser with an excitation photon energy around 6.28 eV (with a 76 MHz repetition rate), a monochromator (1.3 m), and a streak camera with a detection capability ranging from 185 – 800 nm and a time resolution of 2 ps. For the polarization study, PL emission of AlGaN materials with E//c and E⊥c polarization orientations was collected using a polarizer in front of the monochromator.

Our DUV LED material structure is optimized based on the study of *n*- and *p*-AlGaN alloy. The structure is grown on AlN/sapphire substrates by MOCVD. A high quality epilayer of AlN was first grown on (0001) sapphire as a template. A highly conductive *n*-$Al_{0.7}Ga_{0.3}N$ layer of thickness 1.5 µm was then grown on this AlN/sapphire template, followed by AlGaN/AlGaN QW active region and the Mg-doped $Al_{0.7}Ga_{0.3}N$ electron blocking layer. Since it is difficult to achieve a reasonable hole density in an AlGaN alloy with high Al composition, a *p*-$Al_{0.7}Ga_{0.3}N$ layer (10 nm) was employed as an electron blocking layer to effectively block the electron overflow, thereby enhance the electron-hole radiative combination in the QWs. The structure was then completed with a 60 Å Mg doped $Al_{0.5}Ga_{0.5}N$ graded layer and 150 nm heavily Mg doped GaN as the *p*-contact layer.

DUV LEDs with circular geometry (diameter < 300 µm) were fabricated with the *p*-contact in the middle and *n*-contact encompassing the mesa disk to minimize current crowding effect. The fabrication starts from the mesa etching to expose the *n*-AlGaN, followed by Ti/Al/Ti/Au metal deposition and high temperature thermal-annealing to form *n*-contact. Ni/Au was then deposited and annealed to form *p*-contact. Au bumps were deposited by electroplating on *n*- and *p*-contacts. LEDs with different mesa disk sizes were then diced into single devices, flip-chip bonded with Au bumps onto ceramic AlN submount, which was then mounted on to a TO header and heat sink for the measurement. A calibrated integrating optical sphere was used to measure the light output power from the sapphire side. To avoid the optical absorption by the multi-layers on the top (*p*-type AlGaN and GaN, contacts, and the metallic current spreading layer) and the wire bonding pads, the emitted light from a DUV LED grown on the transparent sapphire substrate is commonly extracted through the AlN layer and sapphire substrate by employing flip-chip bonding. Flip-chip architecture is also required for enhanced thermal dissipation.

Integrated sapphire substrate microlens array was incorporated in the UV LED flip-chip architecture to enhance the light extraction efficiency. The schematic diagram is shown in Fig 1. Photoresist reflow and inductive coupling plasma (ICP) dry etching method was used for processing microlens arrays on sapphire substrates. In this method, a thick photoresist layer was spun onto the sapphire substrate and patterned by standard photolithography into cylindrical posts. After baking, the surface tension causes them to take up hemispherical shapes. The preformed resist is then used as a mask for pattern transfer by ICP etching with chlorine-based plasma chemistry. An etch rate of 130 nm/min for sapphire was achieved.

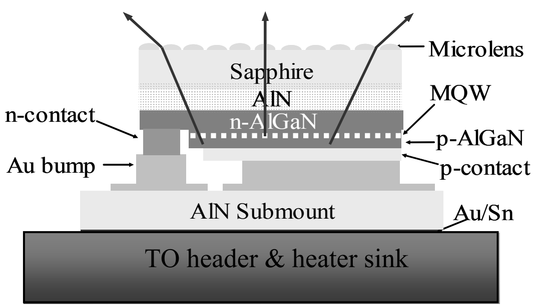


Fig. 1. Schematic diagram of monolithically integrated sapphire microlens array on flip-chip bonded UV LEDs.

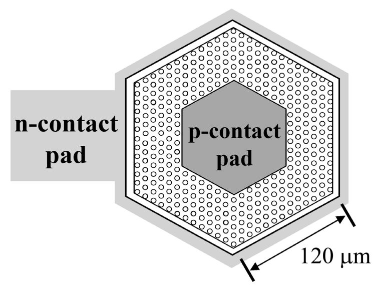


Fig. 2. Schematic diagram of photonic crystal UV LED.

As shown in Fig. 2, photonic crystals (PCs) with triangular lattice patterns of circular holes with varying diameter d = 100 nm to d = 450 nm and periodicity *a* = 300 nm to *a* = 700 nm were fabricated on the LED everywhere (including the metal transparent layer and except the contact pads) using e-beam lithography and ICP dry etching. The UV LED has a hexagonal geometry. The design is guided by the optical pumping configuration that provides a maximum 20-fold enhancement of light extraction by PCs.[9] In the optimized optical pumping configuration, the light generation region (pump spot) was separated from the light extraction region (PCs) and the extraction efficiency was strongly dependent on the angle between the propagation direction of emission light and the PCs lattice structure.

## 3. RESULTS AND DISCUSSIONS

### 3.1 Conductive *n*-AlGaN with high Al content

Conductive *n*-$Al_xGa_{1-x}N$ epilayers with high Al content is used in DUV LED as the bottom cladding layer, and *n*-contact is formed on this layer. A high conductivity is critical to reduce the current crowding effect related with the lateral UV LED geometry. Our group previously reported the properties of MOCVD grown Si-doped *n*-type $Al_xGa_{1-x}N$ alloy with x up to 0.7.[10] A resistivity value of 0.15 Ω cm (with a free electron concentration of $2.1\times10^{18}$ $cm^{-3}$ and mobility of 20 $cm^2$/Vs) was achieved for $Al_{0.65}Ga_{0.35}N$. Achieving highly conductive $Al_xGa_{1-x}N$ alloys with high Al contents is found to be very challenging due to several mechanisms: (i) an increase in the ionization energy of the dopants with increasing Al content;[11] (ii) the formation energy of Al vacancy ($V_{Al}$) decreases with increasing Al content and becomes very low with a triple negatively charged state in AlN ($V_{Al}^{3-}$);[12] (iii) oxygen impurity incorporation as well as the presence of dislocations can enhance the formation of cation vacancies to form energetically stable $V_{Al}$ or $V_{Al}$–$O_{Al}$ complexes.[13] Thus it is critical to control the oxygen impurity and dislocation density.

Here we report the investigation of Si-doped *n*-type $Al_xGa_{1-x}N$ epilayers with x up to 1.[14] The Si dopant concentration ($N_{Si}$) was $3.5 \times 10^{19}$ $cm^{-3}$ in all samples. SIMS measurements indicate that the oxygen concentration in our epilayers is quite low (~ 2 x $10^{17}$ $cm^{-3}$ in AlN). Fig. 3 shows the room temperature Hall measurement results, corresponding to the dependence of resistivity, free electron concentration, and electron mobility on the Al content (x) respectively. A record low room temperature *n*-type resistivity for Al-rich AlGaN alloys have been achieved, specifically, a resistivity of 0.0075 Ω·cm (with an electron concentration of $3.3 \times 10^{19}$ $cm^{-3}$ and mobility of 25 $cm^2/Vs$) has been obtained for $Al_{0.7}Ga_{0.3}N$. We found that the resistivity of *n*-$Al_xGa_{1-x}N$ increases by one order of magnitude when Al content is increased by ~ 8%. This rapid increase in resistivity is predominantly due to an increase in donor ionization energy, which is demonstrated by the activation (ionization) energy $E_0$ dependence on Al content, shown in Fig. 4. $E_0$ increases linearly with an increase of the Al content. This deepening of $E_0$ is due to the fact that with an increase of the Al content in AlGaN alloys, the bandgap and electron effective mass increase, while the dielectric constant and band gap renormalization effect decrease. For pure AlN, an estimated value of $E_0$ of about 120 meV is obtained by extrapolating the experimental data. Taniyasu *et al* estimated the donor ionization energy in AlN of about 85 meV.[15] We believe that the predominant cause for the rapid increase in resistivity of *n*-type $Al_xGa_{1-x}N$ alloys with high Al contents is the Si donor level deepening, and the resistivity of $Al_xGa_{1-x}N$ alloys with high Al contents increases roughly exponentially with the Si donor activation energy. Transport measurement indicates that we have achieved *n*-type conduction in pure AlN with a free electron concentration and mobility of about $1.0 \times 10^{17} cm^{-3}$ and 2 $cm^2/Vs$, respectively. We believe that the *n*-type conductivity values we have achieved here for $Al_xGa_{1-x}N$ alloys (x up to 0.7) are sufficiently high for deep UV emitter applications.

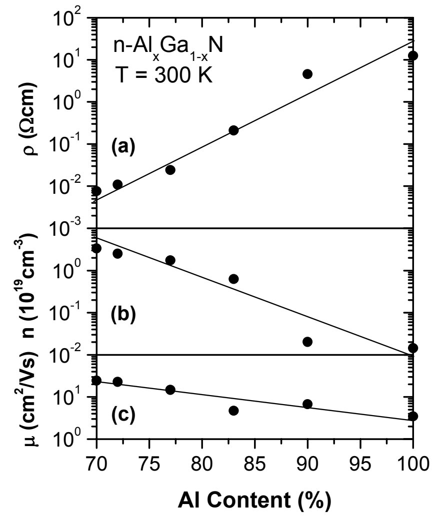


Fig. 3. Room temperature Hall measurement results of *n*-$Al_xGa_{1-x}N$. (a), (b) and (c) show the Al content (x) dependent resistivity, electron concentration, and electron mobility, respectively; lines are guide to the eyes [After Ref. 14].

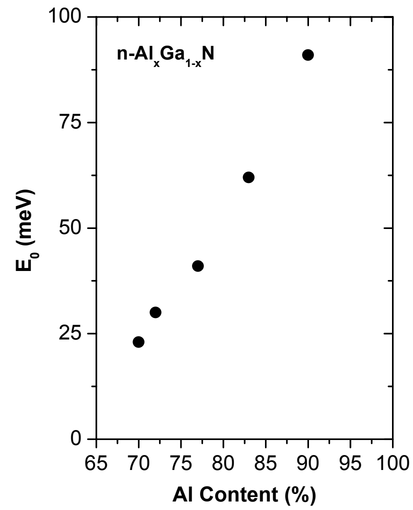


Fig. 4. Si donor activation energy as a function of the Al content, x [After Ref. 14].

### 3.2 Mg doped AlGaN with high Al content

Contrasting with the impressive results of conductive *n*-AlGaN, achieving *p*-AlGaN with high Al content is more challenging due to the large activation energy of the Mg acceptor. Mg doped $Al_xGa_{1-x}N$ with Al content x more than 0.5 have been used in the UV LED as the *p*-cladding layer. However, electrical properties of Mg-doped $Al_xGa_{1-x}N$ alloy with high Al content, especially if it is possible to achieve *p*-type conduction in $Al_xGa_{1-x}N$ alloy with $x>0.5$, is still unclear. We previously reported *p*-type AlGaN for Al content up to 27% [16]as well as optical properties and Mg energy level in the Mg-doped AlN epilayers.[17] From photoluminescence (PL) results, the Mg level in AlN was found to be around 0.5 eV. As the Mg levels in AlGaN deepening with increasing Al content, it is difficult to obtain sufficient free holes. To enhance the hole concentration, several methods have been proposed and explored such as Mg delta doping,[18] short period superlattice (SL) of AlGaN/GaN,[19] and modulation doped AlGaN/GaN SL.[20] Due to the low conductivity of *p*-type AlGaN alloys, hole injection efficiency is the most serious problem in DUV LEDs.

In the DUV LED structure, one of the crucial layers is the electron blocking layer. It plays an important role in blocking the electrons from getting into the p-layer region and thus enhancing the carrier recombination in the active region and hence the emission efficiency. However, a low quality blocking layer could introduce long wavelength emission components in DUV LEDs when injected electrons overflow to the p-region. Furthermore, the quality of the electron blocking layer affects profoundly holes injection into the active region. Understanding and improving the material quality and conductivity of Mg-doped AlGaN alloys are essential to improve the DUV LED performance.

Mg-doped $Al_{0.7}Ga_{0.3}N$ epilayers of thickness ~ 1 μm were grown on AlN/sapphire templates by metal organic chemical vapor deposition (MOCVD). An AlN epilayer of thickness ~ 0.5 μm was first grown on sapphire (0001) substrate and followed by the growth of Mg-doped $Al_{0.7}Ga_{0.3}N$ epilayer. As-grown epilayers were highly resistive and post growth rapid thermal annealing was done to activate Mg acceptors. Ni/Au was used as contacts in the standard Van der Pauw configuration for Hall effect measurements. The resistivity obtained at room temperature is about $10^5$ Ωcm (semi-insulating). Fig. 5 shows the variation of resistivity with temperature in the range between 450 and 800 K of a typical Mg-doped $Al_{0.7}Ga_{0.3}N$ epilayer.[21] The resistivity decreases exponentially with increasing temperature. At high temperatures (> 700 K), it shows consistently a signature of *p*-type conduction. At 800 K, the measured *p*-type resistivity is about 40 Ωcm. The activation energy of Mg acceptor is first estimated by using the following equation

$$\rho(T) = \rho_0 \, e^{E_A / kT} \qquad (1)$$

Where $\rho$(T) is the resistivity at temperature T, and $E_A$ is the activation energy of Mg acceptor. Inset of Fig. 5 shows the Arrhenius plot of the resistivity vs T. The fitted value of $E_A$ is about 320 meV. To obtain $E_A$ more accurately, $E_A$ is also estimated by including the temperature dependence of the mobility at high temperatures ($\mu \propto T^{-3/2}$). The fitted $E_A$ value increased to 396 meV, which is close to the previously estimated value by extracting Mg levels between GaN and AlN.[18] With this result, we can now estimate the theoretical limit of the resistivity of Mg-doped Al-rich $Al_xGa_{1-x}N$ alloys.

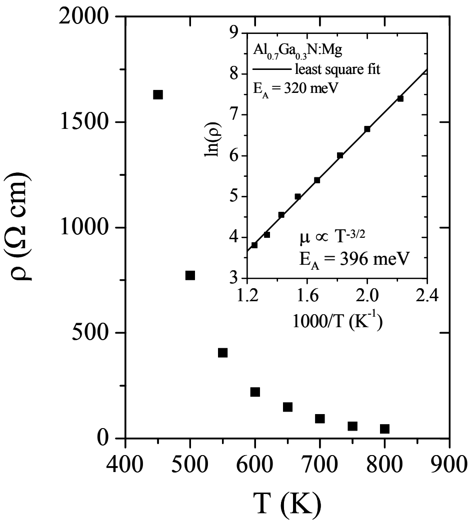


Fig. 5. Temperature variation of resistivity of the Mg-doped $Al_{0.7}Ga_{0.3}N$ epilayer in the temperature range of 450 - 800 K. Inset is the Arrhenius plot of ρ vs T. The solid line is the least square fit of data with Eq. (1). The fitted value of $E_A$, is 320 meV (396 meV) without (with) considering the variation of μ with T ($\mu \propto T^{-3/2}$). [After Ref. 21].

The resistivity of $Al_{0.7}Ga_{0.3}N$:Mg is thus (see Ref. 21)

$$\rho\,(Al_{0.7}Ga_{0.3}N:Mg) \approx (3 \sim 10)\,\rho\,(GaN:Mg) \exp\left\{\frac{\Delta E_A}{kT}\right\} \qquad (2)$$

Using typical values for p-GaN, $E_A$ = 160 meV and $\rho$ = 1 Ωcm (at room temperature), we have the room temperature resistivity

$$\rho(Al_{0.7}Ga_{0.3}N:Mg) \approx (3 \sim 10) e^{236meV/kT} \approx (3 \sim 10) e^{236meV/25meV} \approx (4 \sim 13) \times 10^4 \ \Omega cm \qquad (3)$$

Thus $\rho$ is in the range of (4 ~ 13) x $10^4$ Ω cm (semi-insulating) at room temperature for Mg-doped $Al_{0.7}Ga_{0.3}N$ alloys. The resistivity we obtained for $Al_{0.7}Ga_{0.3}N$:Mg is in the range of the estimated value by Eq. (3). Taking into account of the hole mobility variation with temperature ($\mu_p \propto T^{-3/2}$), the resistivity of $Al_{0.7}Ga_{0.3}N$:Mg at 800 K is estimated from Eq. (3) to be in the range of (9 ~ 30) Ω cm as a lower limit, which is consistent with our measured value at 800 K (40 Ω cm).

Now, let us discuss the effect of this Mg-doped $Al_{0.7}Ga_{0.3}N$ electron blocking layer to the performance of DUV LEDs. Typically the thickness of the blocking layer is about 5 - 10 nm. For a standard size of 300 μm x 300 μm LED, the resistance of this layer is

$$R = \rho \frac{l}{A} = (4 \sim 13) \times 10^4 \Omega\, cm \frac{(5 \sim 10)\ nm}{300\,\mu m \times 300\,\mu m} \approx (22 \sim 130)\ \Omega \qquad (4)$$

The voltage drop across this layer at 20 mA current (at forward bias $V_f$) is between 0.5 ~ 2.6 V. Although this electron blocking layer is semi-insulating at room temperature, the potential drop at this layer is still relatively small due to the fact that only a very thin layer (5-10 nm) is needed. This fact explains why the DUV LEDs are still performing reasonably well using high Al-content AlGaN:Mg as electron blocking layers.[22,23]

In summary, we have grown Mg-doped $Al_{0.7}Ga_{0.3}N$ epilayers with improved quality by MOCVD. Electrical and optical properties of the epilayers were studied. We obtained a resistivity around $10^5$ Ωcm at 300 K and a *p*-type resistivity of about 40 Ωcm at 800 K. The energy level of Mg was estimated to be around 400 meV for $Al_{0.7}Ga_{0.3}N$ epilayer from the temperature dependence of the resistivity. Fundamental limit of *p*-type conductivity of Mg-doped Al-rich $Al_xGa_{1-x}N$ alloys was also addressed.

### 3.3 DUV LED devices

Based on the study of *n*- and *p*-AlGaN, we optimized the DUV LED structure, grown on AlN/sapphire substrates by MOCVD. As shown in Fig. 6(a), a high quality epilayer of AlN was first grown on (0001) sapphire as a template. A highly conductive *n*-$Al_{0.7}Ga_{0.3}N$ layer of thickness 1.5 µm was then grown on this AlN/sapphire template, followed by AlGaN/AlGaN QW active region and the Mg-doped $Al_{0.7}Ga_{0.3}N$ electron blocking layer. Since it is difficult to achieve a reasonable hole density in an AlGaN alloy with high Al composition, a *p*-$Al_{0.7}Ga_{0.3}N$ layer (10 nm) was employed as an electron blocking layer to effectively block the electron overflow, thereby enhance the electron-hole radiative recombination in the QWs. The structure was then completed with a 60 Å Mg doped $Al_{0.6}Ga_{0.4}N$ graded layer and 150 nm heavily Mg doped GaN as the *p*-contact layer. Small-dimension circular LEDs with diameter < 300 µm have a better current spreading as well as small thermal resistance. Large-size LEDs with interdigital shape are also fabricated to overcome the current crowding effect. Fig 6(b) is the fabricated device image, and Fig 6(c) is the flip-chip bonded device mounted on TO-66 head with 280 nm light emission.

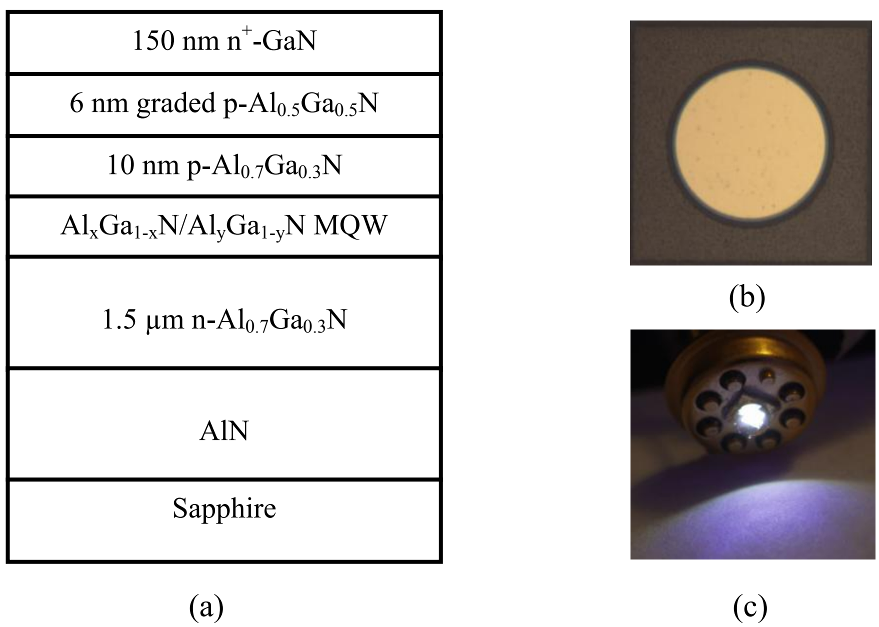


Fig. 6. (a) Schematic diagram of DUV LED material structure. (b) Optical image of circular DUV LED device. (c) Image of flip-chip bonded DUV LED mounted on TO-66 head with 280 nm light emission.

Fig. 7(a) shows the electroluminescence (EL) spectrum of a 280 nm deep UV LED with a 300 µm diameter size under 40 mA dc current. The inset of Fig. 7 shows the I-V characteristic of 280 nm deep UV LEDs. The forward voltage, $V_F$, of 6.7 V is observed at 20 mA current. We believe that with further optimization of *n*- and *p*-contact annealing, $V_F$ can be further reduced. Fig. 7(b) shows the L-I characteristic of the same device. We have achieved an optical power output of 0.35 mW and a power density of 0.48 W/cm$^2$ at 20 mA (while the maximum optical power and power density are 1.1 mW and 1.5 W/cm$^2$, respectively). With the incorporation of the optimized growth condition of the electron blocking layer, we observed enhancement in the DUV LED output power. The long wavelength components were significantly reduced in the EL spectrum. We believe the improved material quality of the electron blocking layer played an important role in suppressing the long wavelength components in the EL spectrum. Further improvement of the conductivity of Mg-doped AlGaN epilayer is required to further enhance the efficiency and performance of DUV LEDs, especially when shorter wavelength emission is required.

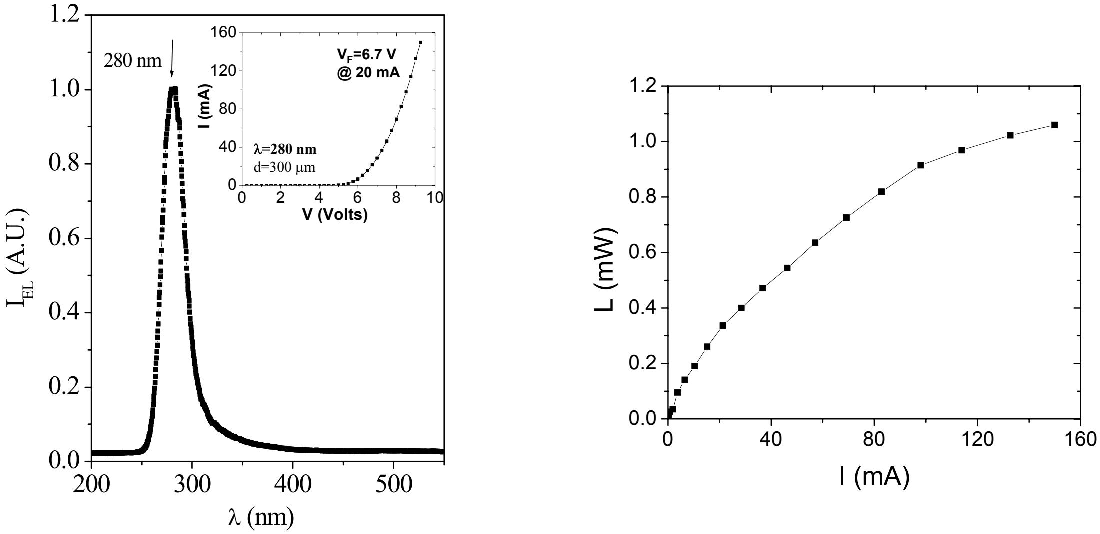


Fig. 7. (a) EL spectrum of a disk shape (d = 300 μm) deep UV LED with peak emission at 280 nm under DC bias (I = 40 mA). Inset is the I-V characteristic of the same 280 nm UV LED. (b) Light output power versus current (L-I) of the same device.

### 3.4 DUV LED with integrated microlens array

To reduce the problem of light trapping in the high refractive index semiconductor layers, here we demonstrate that integrated sapphire substrate microlens in conjunction with flip-chip bonding can be used to improve the light extraction. Microlense has been widely used for light collimation and coupling in the optical systems.[24] In recent years, monolithically integrated microlenses fabricated on the GaN and AlN surfaces or its sapphire substrate surface have also been reported for the similar purposes.[25] Here we report the flip-chip bonded 280 nm DUV LED with integrated sapphire substrate microlens array, and the results demonstrate that microlense array is also an efficient method to enhance the light extraction for UV LEDs.[26]

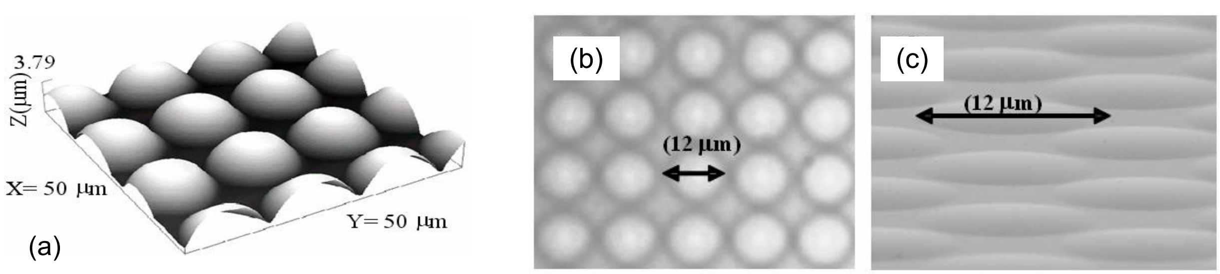


Fig. 8. (a) AFM image of photoresist after reflow. (b) Optical microscope image and (c) SEM image of a fabricated sapphire microlens array. (After Ref. 26).

Photoresist reflow and ICP etching was used for processing microlens arrays on sapphire substrates. In this method, a thick photoresist layer was spun onto the sapphire substrate and patterned by standard photolithography into cylindrical posts. After baking, the surface tension causes them to take up hemispherical shapes, shown by the atomic force microscope (AFM) image in Fig. 8(a). The preformed resist is then used as a mask for pattern transfer by dry etching. The optical microscope image (Fig. 8(b)) and the scanning electron microscope (SEM) image (Fig. 8(c)) show the fabricated microlens array on sapphire substrate. The fabricated microlens has a bottom diameter of 12 μm and a height of 1 μm with a pitch of 20 μm. To study the effect of microlens array, two representative devices diced from the nearby locations from the same processed wafer with/without microlens formation are characterized and compared with each other. The angular distribution of light measurement shows the light emission pattern from the sapphire substrate has no significant difference with and without microlens array. This is understandable since the microlens has a size much smaller than the LED dimension. The change in the directionality of the LED emission caused by individual microlens is smeared out. To compare the light extraction efficiency, the light emission was measured with a UV-enhanced Si detector on top of LED with a fixed distance, and the relative emission power of the LED with and without microlens array are plotted in Fig. 9. The results clearly show that the LED with microlens array produces more light output than that of without microlens. Specifically, a 55% increase in the output power is measured at 20 mA DC current driving. The enhanced light extraction is attributed to the curvature surface profile of the microlens.

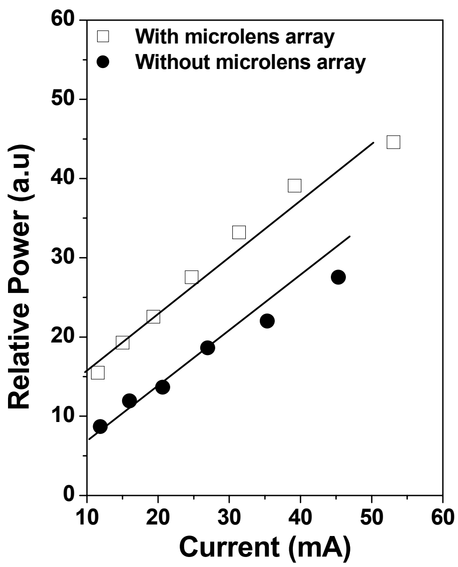


Fig. 9. Comparison of the DUV LED output power with and without the microlens array. A 55% increase in the optical output power by the microlens array formation was measured at 20 mA DC driving. (After Ref. 26).

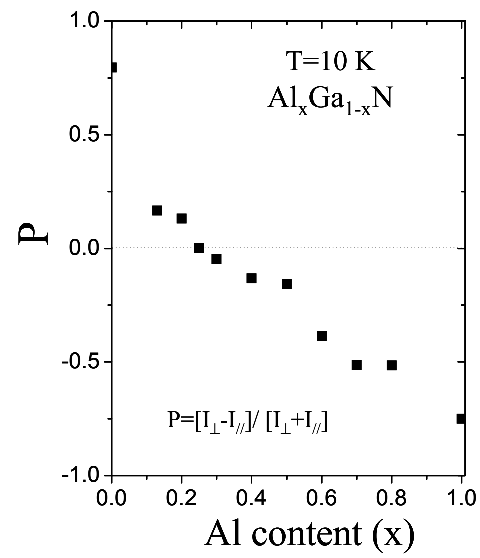


Fig. 10. The degree of polarization $P$ vs. x in $Al_xGa_{1-x}N$ alloys. (After Ref. 27)

### 3.5 Polarization study of AlGaN material[27]

From measurements of PL emission intensity along the directions of parallel ($I_{//}$) and perpendicular ($I_{\perp}$) to the crystal $c$ axis, the degree of polarization $P$, defined by $P=(I_{\perp}-I_{//})/(I_{\perp}+I_{//})$, of AlGaN epilayer is obtained, as shown in Fig. 10. Polarization decreases almost linearly with increasing Al content (x), and $P = 0$ at x = 0.25. This phenomenon is caused by the difference of valence band structure of GaN and AlN.[8] Briefly speaking, the crystal field causes a negative splitting in AlN valence band and a positive splitting in GaN. As a consequence, the top valence band of AlN has $\Gamma_7$ symmetry, while it is $\Gamma_9$ for GaN. Therefore, the light emission due to recombination of electron and hole is polarized with $E//c$ for AlN and $E\perp c$ for GaN. For AlGaN alloy, the polarization depends on Al concentration.

The polarization of light emission from AlGaN has a profound influence on the DUV LED external efficiency. As shown in Fig. 11 with a diagram structure of a general QW LED, the light extraction is limited to a small cone, defined by the refractive index contrast between the semiconductor material and the environment (air or encapsulation). Typically, this cone is about ~ 20$^o$. Only the photons emitted in this cone (propagating toward the outlet of the cone) can be extracted, while others form guided wave in the cladding layer, and finally are absorbed by the semiconductor defects. For most semiconductor materials covering infrared to blue wavelength, the polarization of the emitted light is mainly parallel to the surface plane, i.e. the propagation of the light is toward the surface, as shown in Fig 11(b), so the emitted photons in the cone can be extracted. However, for AlGaN-based DUV LED with Al composition more than 25%, the emitted light has a polarization perpendicular to the surface plane; hence, most light propagate and is confined in the semiconductor layer, as shown in Fig. 11(c).

To enhance the transverse light extraction in UV LEDs, deep surface features should be introduced into the cladding and QW layers so that the transverse light can cross these surface features. Of the different schemes, photonic crystal (PC) is a very promising technique to significantly enhance LED light extraction efficiency.

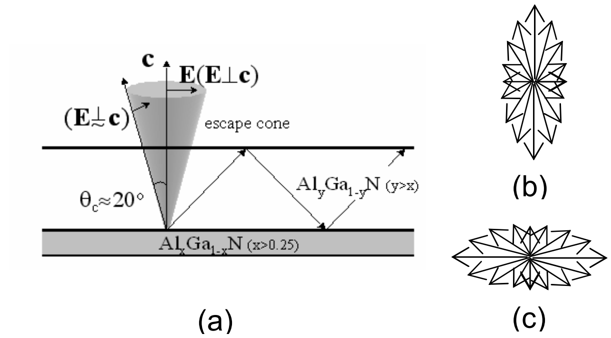


Fig. 11. Schematic diagrams of (a) light extraction cone of LEDs, and (b) and (c) of light propagation direction caused by different polarization.

### 3.6. UV LEDs with photonic crystal structure[28]

Using electron beam lithography and ICP plasma etching, triangular arrays of holes with different diameters/periodicities were etched on the UV LEDs into QW region. Fig. 12 (a) and (b) show the SEM images after the patterns were etched with lattice constant *a* = 180 nm, hole diameter *d* = 100 nm and *a* = 300 nm, *d* = 120 nm respectively. AFM measurement revealed that the depth of the etched holes varied from 175 nm to 190 nm and that the holes with larger diameter were etched relatively deeper. This indicates that most of the holes were etched through to the active layer.

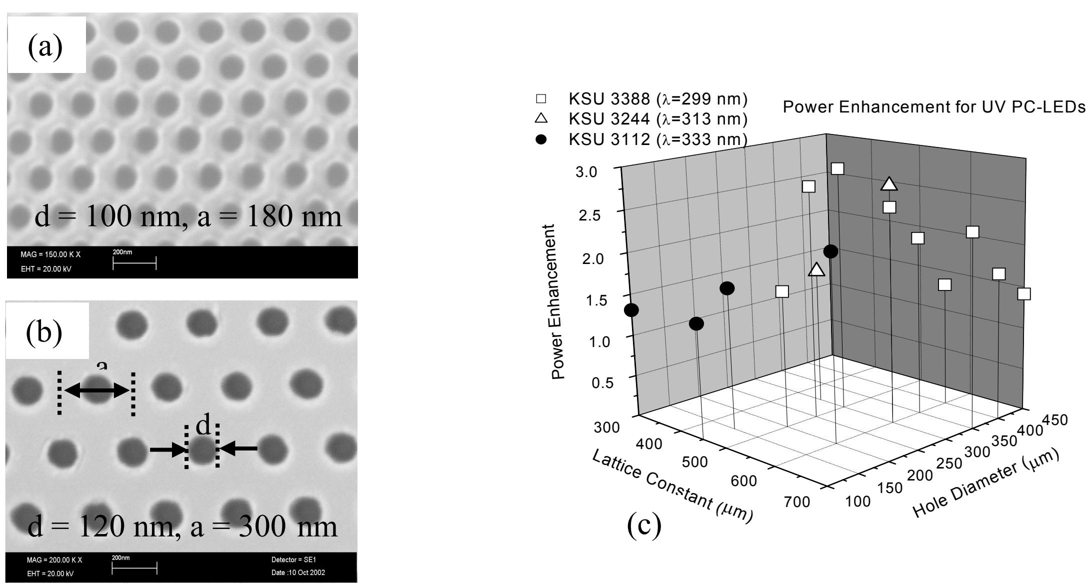


Fig. 12. SEM images of nitride photonic crystals (a) with *a* = 180 nm, *d* = 100 nm, (b) with *a* = 300 nm, *d* = 120 nm. In (c), 3D plot of the PCs lattice constant *a* and the air hole diameter *d* dependence of the power enhancement factor in the UV LEDs. Three different sets of UV LEDs were studied. A highest enhancement factor of about 2.9 was observed with PCs parameters *a* = 500 nm, *d* = 300 nm. (After Ref.28).

## 4. SUMMARY

Of the many challenges for AlGaN-based DUV LEDs, here we addressed some fundamental issues, including *n*- and *p*-conductivity of AlGaN with Al content more than 70%, and light extraction efficiency. For Si doped $Al_{0.7}Ga_{0.3}N$, a room temperature *n*-type resistivity as low as 0.0075 Ω·cm has been achieved. For Mg doped $Al_{0.7}Ga_{0.3}N$, we have obtained a resistivity around $10^5$ Ω cm at room temperature and confirmed p-type conduction at elevated temperatures (> 700 K) with a resistivity of about 40 Ω cm at 800 K. With the optimized material structure, 280 nm DUV LED with forward voltage of 6.7 V, and output power of 0.35 mW has been achieved at 20 mA. We integrated sapphire microlens array (with a bottom diameter 12 μm) on flip-chip bonded UV LED substrates, and a light extraction enhancement of 55% was achieved due to the microlens surface curvature. Polarization study shows that for $Al_xGa_{1-x}N$ with x>0.25, the transverse light is the dominant emission in AlGaN materials; to improve the transverse light extraction, photonic crystal structures were incorporated into the devices. We have achieved the nanofabrication of triangular lattice array of photonic crystals with diameter/periodicity as small as 100/180 nm on UV LEDs, and initial results show significant light extraction enhancement can be obtained. We believe that with further improvement in the design and nano-fabrication of photonic crystal structures, greater enhancement is expected.

## ACKNOWLEDGEMENT

Our research program is supported by grants from ARO, NSF, DOE, and DARPA. This invited paper is a collection of contributions from our group members: M. L. Nakarmi, K. H. Kim, K. B. Nam, J. Shakya, J. Li, N. Nepal, T. N. Order, K. Zhu, S. X. Jin, M. Khizar, and W. P. Zhao.

## REFERENCES

[1] http://www.darpa.mil/mto/suvos/
[2] V. Adivarahan, W. H. Sun, A. Chitnis, M. Shatalov, S. Wu, H. P. Maruska, and M. Asif Khan, *Appl. Phys. Lett*., **85**, 2175 (2004).
[3] T. Nishida, H. Saito, and N. Kobayashi, *Appl. Phys. Lett*. **78**, 399 (2001).
[4] A. Chitnis, J. P. Zhang, V. Adivarahan, W. Shuai, J. Sun, M. Shatalov, J. W. Yang, G. Simin, and M. Asif. Khan, *Jpn. J. Appl. Phys*. **41**, L450 (2002).
[5] C. Chen, V. Adivarahan, J. Yang, M. Shatalov, E. Kuokstis, and M. A. Khan, *Jpn. J. Appl. Phys*. **42**, L1039 (2003).
[6] C.G. Van de Walle and J. Neugebauer, *J. Appl. Phys.* **95**, 3851 (2004).
[7] T. Mattila and R.M. Nieminen, *Phys. Rev. B*. **55**, 9571 (1997).
[8] J. Li, K.B. Nam, M. L. Nakarmi, J.Y. Lin, H.X. Jiang, P. Carrier, and S.H. Wei, *Appl. Phys. Lett*. **83**, 5163 (2003).
[9] T. N. Oder, J. Shakya, J. Y. Lin, and H. X. Jiang, *Appl. Phys. Lett.* **83,** 1231, (2003).
[10] K. B. Nam, J. Li, M. L. Nakarmi, J. Y. Lin, and H. X. Jiang, *Appl. Phys. Lett*. **81**, 1038 (2002).
[11] B. Jahnen, M. Albrecht, W. Dorsch, S. Christiansen, H. P. Strunck, D. Hanser, and R. F. Davis, *MRS Internet J. Nitride Semicond. Res.* **3**, 39 (1998).
[12] C.G. Van de Walle and J. Neugebauer, *J. Appl. Phys.* **95**, 3851 (2004).
[13] J. Oila, J. Kivioja, V. Ranki, K. Saarinen, D.C. Look, R.J. Molnar, S.S. Park, S.K. Lee, and J.Y. Han, *Appl. Phys. Lett*. **82**, 3433 (2003).
[14] M. L. Nakarmi, K. H. Kim, K. Zhu, J. Y. Lin, and H. X. Jiang, *Appl. Phys. Lett*. **85**, 3769 (2004).
[15] Y. Taniyasu, M. Kasu, and N. Kobayasu, *Appl. Phys. Lett*. **81**, 1255 (2002).
[16] J. Li, T. N. Oder, M. L. Nakarmi, J. Y. Lin, and H. X. Jiang. *Appl. Phys. Lett*. **80**, 1210 (2002).
[17] K. B. Nam, M. L. Nakarmi, J. Li, J. Y. Lin, and H. X. Jiang. *Appl. Phys. Lett*. **83**, 878 (2003).
[18] M. L. Nakarmi, K. H. Kim, J. Li, J. Y. Lin, and H. X. Jiang. *Appl. Phys. Lett*. **82**, 3041 (2003).
[19] A.Saxler, W. C. Mitchel, P. Kung, and M. Razeghi, *Appl. Phys. Lett*. **74**, 2023 (1999).
[20] E. L. Waldron, J. W. Graff, and E. F. Schubert, *Appl. Phys. Lett*. **79**, 2737 (2001).
[21] M. L. Nakarmi, K. H. Kim, M. Khizar, Z. Y. Fan, J. Y. Lin, and H. X. Jiang, *Appl. Phys. Lett*., **86**, 092108 (2005).
[22] V. Adivarahan, S. Wu, J. P. Zhang, A. Chitnis, M. Shatalov, V. Mandavilli, R. Gaska, and M. Asif Khan, *Appl. Phys. Lett.* **84**, 4762 (2004).
[23] A. Yasan, R. McClintock, K. Mayes, D. Shiell, L. Gautero, S. R. Darvish, P. Kung, and M. Razeghi, *Appl. Phys. Lett*. **83**, 4701 (2003).

[24] A. W. Lohmann, *Appl. Opt.* **28**, 4996 (1989).
[25] T. N. Order, J. Shakya, J. Y. Lin, and H. X. Jiang, *Appl. Phys. Lett*. **82**, 3692 (2003).
[26] M. Khizar, Z. Y. Fan, K. H. Kim, J. Y. Lin, and H. X. Jiang, *Appl. Phys. Lett*., **86**, 173504 (2005).
[27] K. B. Nam, J. Li, M. L. Nakarmi, J. Y. Lin, and H. X. Jiang, *Appl. Phys. Lett*., **84**, 5264 (2004).
[28] J. Shakya, K. H. Kim, T. N. Oder, J. Y. Lin, and H. X. Jiang, *Proc. SPIE*, **5530**, 241 (2004).